

## Variation of copper isotopes in chalcopyrite from Dabu porphyry Cu-Mo deposit in Tibet and implications for mineral exploration

Song Wu<sup>a</sup>, Youye Zheng<sup>a,b,\*</sup>, Da Wang<sup>a</sup>, Huifang Chang<sup>a</sup>, Meng Tan<sup>a</sup>

<sup>a</sup> State Key Laboratory of Geological Processes and Mineral Resources, School of Earth Science and Resources, China University of Geosciences, Beijing, China

<sup>b</sup> State Key Laboratory of Geological Processes and Mineral Resources, Faculty of Earth Resources, China University of Geosciences, Wuhan 430074, China



### ARTICLE INFO

#### Keywords:

Cu isotope variation  
Mineral exploration  
Porphyry deposit  
Dabu  
Southern Tibet

### ABSTRACT

The study presents copper (Cu) isotope data of mineral separates of chalcopyrite from four drill core samples in the Miocene Dabu porphyry Cu-Mo deposit formed in a post-collisional setting in the Gangdese porphyry copper belt, southern Tibet. Copper isotope values in hypogene chalcopyrite range from  $-1.48\text{\textperthousand}$  to  $+1.12\text{\textperthousand}$ , displaying a large variation of up to  $2.60\text{\textperthousand}$ , which demonstrates Cu isotope fractionation at high-temperature during hydrothermal evolution. The majority of measured chalcopyrite isotopic compositions show a gradual increasing trend from  $-1.48\text{\textperthousand}$  to  $+1.12\text{\textperthousand}$  with the increase of drilling depth from 130 m to 483 m, as the alteration assemblages change from potassic to phyllitic. Similarly, the other  $\delta^{65}\text{Cu}$  values ( $\delta^{65}\text{Cu} = ((^{65}\text{Cu}/^{63}\text{Cu})_{\text{sample}}/(^{65}\text{Cu}/^{63}\text{Cu})_{\text{standard}} - 1) \times 1000$ ) of the chalcopyrite show a gradual increasing trend from  $-1.48\text{\textperthousand}$  to  $+0.59\text{\textperthousand}$  with the decrease of drilling depth from 130 m to 57 m, as the alteration assemblages change from potassic, phyllitic, through argillitic to relatively fresh. These observations suggest a genetic link between Cu isotope variation and silicate alteration assemblages formed at different temperatures, indicative of a Rayleigh precipitation process resulting in the large variation of  $\delta^{65}\text{Cu}$  values at Dabu. In general, samples closest to the center of hydrothermal system dominated by high-temperature potassic alteration are isotopically lighter, whereas samples dominated by low-temperature phyllitic alteration peripheral to the center are isotopically heavier. The predicted flow pathways of hydrothermal fluids are from No. 0 to No. 3 exploration line, and the lightest  $\delta^{65}\text{Cu}$  values are the most proximal to the hydrothermal source. Finally, we propose that the northwest side of the No. 0 exploration line has high potential for hosting undiscovered orebodies. The pattern of Cu isotope variation in conjunction with the features of silicate alteration in porphyry system can be used to trace the hydrothermal flow direction and to guide mineral exploration.

### 1. Introduction

Copper is the first-row transition metal element with two stable isotopes of  $^{65}\text{Cu}$  and  $^{63}\text{Cu}$  that have average abundances of 69.17 and 30.83%, respectively (Lodders, 2003). With the improvement of multi-collector-inductively coupled plasma-mass spectrometry (MC-ICP-MS) techniques, copper isotope analytical precision has been significantly improved (Maréchal et al., 1999; Zhu et al., 2000; Liu et al., 2014a; Sossi et al., 2015), allowing Cu isotope to be used to trace metal contaminants in the environment (Bigalke et al., 2010; El Azzi et al., 2013) or to evaluate biogeochemical cycling (Weinstein et al., 2011; Jouvin et al., 2012; Liu et al., 2014b), and as indicators of redox reactions (Markl et al., 2006; Asael et al., 2012; Lv et al., 2016) or mineral exploration in ore deposits (Mathur et al., 2009, 2012; Braxton and Mathur, 2011; Duan et al., 2015). Copper isotope ratios can be significantly fractionated during a variety of low-temperature processes,

including (1) redox reactions, (2) mineral dissolution and precipitation, (3) sorption of aqueous  $\text{Cu}^{2+}$  onto mineral and bacterial surfaces, and (4) biological activity (Huang et al., 2016 and references therein). In contrast, during high-temperature rock forming processes, it is widely accepted that the Cu isotope fractionation is insignificant or small, and characterized by restricted range of  $\delta^{65}\text{Cu}$  values for bulk silicate Earth (BSE), mainly due to small mass difference between Cu isotopes ( $-0.14\text{\textperthousand}$  to  $+0.26\text{\textperthousand}$ ; Zhu et al., 2000; Luck et al., 2003; Ben Othman et al., 2006; Li et al., 2009; Liu et al., 2015). However, other studies (Larson et al., 2003; Graham et al., 2004; Maher and Larson, 2007; Li et al., 2010; Maher et al., 2011) have demonstrated that significant Cu isotopic variations (up to 4%) actually occur at some high temperature (hypogene) ore deposits during magmatic and hydrothermal processes. For instance, systematic Cu isotopic variations within high-temperature hypogene mineralization ( $>2\text{\textperthousand}$ ) have been found in the Northparkes porphyry Cu-Au deposit, which are characterized by a sharp down-hole

\* Corresponding author at: State Key Laboratory of Geological Processes and Mineral Resources, School of Earth Science and Resources, China University of Geosciences, Beijing, China.  
E-mail address: [zhyouye@163.com](mailto:zhyouye@163.com) (Y. Zheng).

decrease from the low-grade peripheral alteration zones (phyllitic-propylitic alteration zone) to the margins of the most mineralized zones (Li et al., 2010). Experimental studies also indicate that significant isotopic fractionation in hypogene ore-forming systems depends on the pH of the mineralizing fluid and the controls over partitioning of Cu between a vapor and liquid phase (Maher et al., 2011). These observations show the potential utility of Cu isotopes to identify the mineralized center of a hydrothermal system and guide mineral exploration, because of the preliminary studies of fractionation behaviors of Cu isotopes in high-temperature ore-forming environments (e.g., Mathur et al., 2013; Yao et al., 2016).

The Dabu deposit, located in the southern Lhasa terrane, is one medium-sized porphyry Cu–Mo deposit formed in a post-collisional setting in Tibet, in which the supergene enrichment zone and leach cap are not developed. The orebody in this deposit is centered on a single monzogranite porphyry with only one mineralization event during the Miocene (Wu et al., 2014, 2016), so Cu isotope variation due to multiple stages of intrusive activity and mineralization can be ruled out. To date, further reserves have not been identified at the Dabu deposit when compared with Qulong and Zhunuo porphyry deposits in the Gangdese porphyry copper belt, which may reflect imprecise knowledge of the center of the hydrothermal system. In this study, we present Cu isotope data of chalcopyrite separates from samples taken from four drill holes in the Dabu porphyry Cu–Mo deposit. We discuss high-temperature Cu isotope fractionation related to fluid evolution, and we provide potential insights to assist further exploration at Dabu.

## 2. Geological setting and deposit geology

The Gangdese belt is one of the most richly endowed copper provinces in the Alpine-Himalayan orogen (Fig. 1a; Hou et al., 2011; Mao et al., 2014). This belt includes the Qulong porphyry Cu–Mo deposit (Fig. 1b), which was first described by Zheng et al. (2004), and is now the largest porphyry copper deposit in China with resources of > 10 Mt Cu at 0.44 wt% Cu and 0.44 Mt Mo at 0.02 wt% Mo (Zheng et al., 2015). There are also some Miocene-age porphyry deposits in this belt such as the large and medium sized Zhunuo, Jiru and Tangbula deposits

(Fig. 1b; Wang et al., 2010; Zheng et al., 2014a,b; Sun et al., 2017). The magmatism (Fig. 1b) occurring in this belt is expressed by the regionally extensive Jurassic to Eocene Gangdese batholith, which is genetically related to the subduction of and subsequent break-off a Neo-Tethys oceanic slab (Wen et al., 2008; Ji et al., 2009), the Paleocene to Eocene Linzizong volcanic succession (Mo et al., 2008; Lee et al., 2012) and Oligocene to Miocene adakite-like granitoid rocks (Chung et al., 2009; Zheng et al., 2012; Sun et al., 2013) resulting from the collision and subsequent convergence of the Indian and Asian plates.

The Dabu deposit lies about 40 km west of Lhasa (Fig. 1b), with a reserve of approximately 0.5 Mt Cu at ~ 0.31 wt% Cu (Zheng et al., 2015). The ore minerals consist of disseminated and veined chalcopyrite, pyrite, and molybdenite hosted in a monzogranite porphyry that was subjected to potassic and phyllitic alteration. The Miocene monzogranite porphyry and granodiorite occur as small stocks or dikes that were emplaced into Eocene medium-coarse grained biotite monzogranite and porphyritic monzogranite (Fig. 2). The age of mineralization constrained by Re-Os isochron dating of molybdenite is  $14.8 \pm 0.2$  Ma (Qu et al., 2007), which overlaps the age ( $14.6 \pm 0.4$  Ma) of ore-bearing monzogranite porphyry obtained by U-Pb SHRIMP dating of zircon (Wu et al., 2014). The mineralization process at the Dabu deposit can be divided into three stages of veining, namely stage I quartz-K-feldspar (biotite) ± chalcopyrite ± pyrite, stage II quartz-molybdenite ± pyrite ± chalcopyrite, and stage III quartz-pyrite ± molybdenite (Wu et al., 2017a). Fluid inclusion studies suggest that the ore-forming fluids at the Dabu deposit were high temperature (244–486 °C) and high salinity (1.1–55.8 wt% NaCl equiv.), and were derived from a H<sub>2</sub>O–NaCl magmatic–hydrothermal system (Wu et al., 2017a). Alteration in the Dabu deposit is mainly dominated by potassic, phyllitic and propylitic assemblages. Potassic alteration is characterized by disseminated fine-grained secondary K-feldspar crystals and thin flakes of secondary biotite. Phyllitic alteration is mainly dominated by sericitic that locally replaced plagioclase and white phyllitic alteration halos, whereas the propylitic alteration is characterized by weakly developed chlorite and epidote.

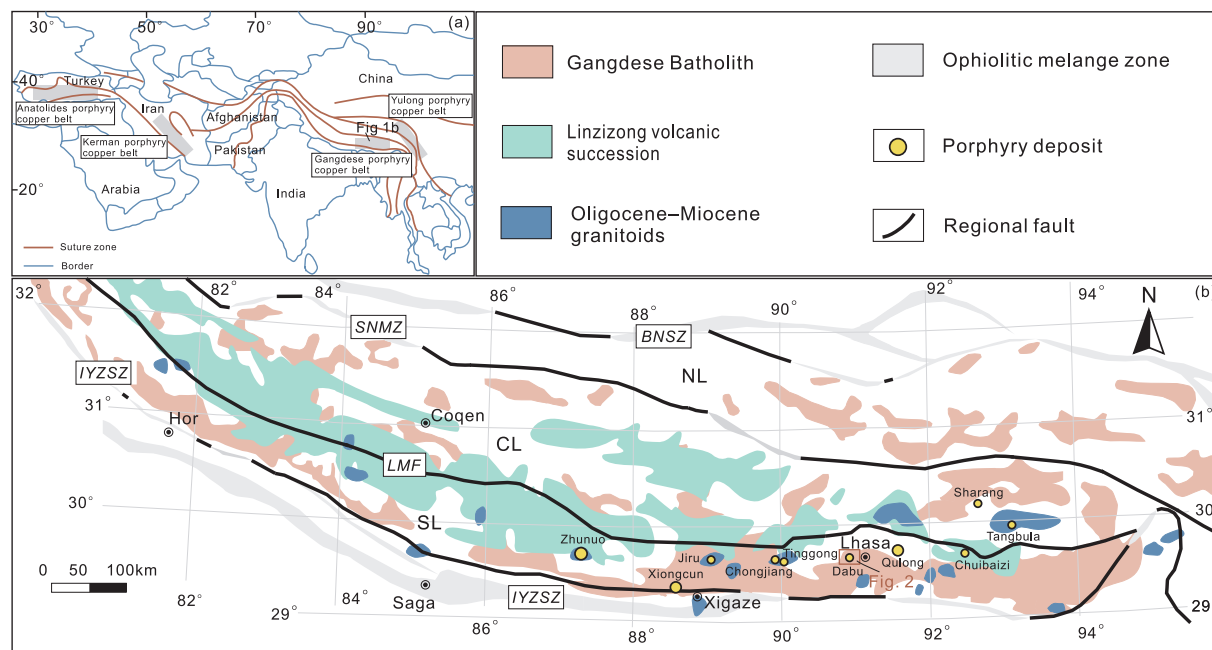


**Fig. 1.** (a) Distribution of some collision-related porphyry copper belts in the Alpine-Himalayan orogenic belt (modified after Singer et al., 2005 and Hou et al., 2011); (b) Simplified geological map of the Lhasa terrane showing the distribution of main porphyry deposits and locality of the study area (Wu et al., 2016). Abbreviations: BNSZ = Bangong–Nujiang suture zone, SNMZ = Shiquan River–Nam Tso Mélange Zone, LMF = Luobadui–Milashan Fault, IYZSZ = Indus–Yarlung Zangbo Suture Zone, SL = southern Lhasa Terrane, CL = central Lhasa Terrane, NL = northern Lhasa Terrane.

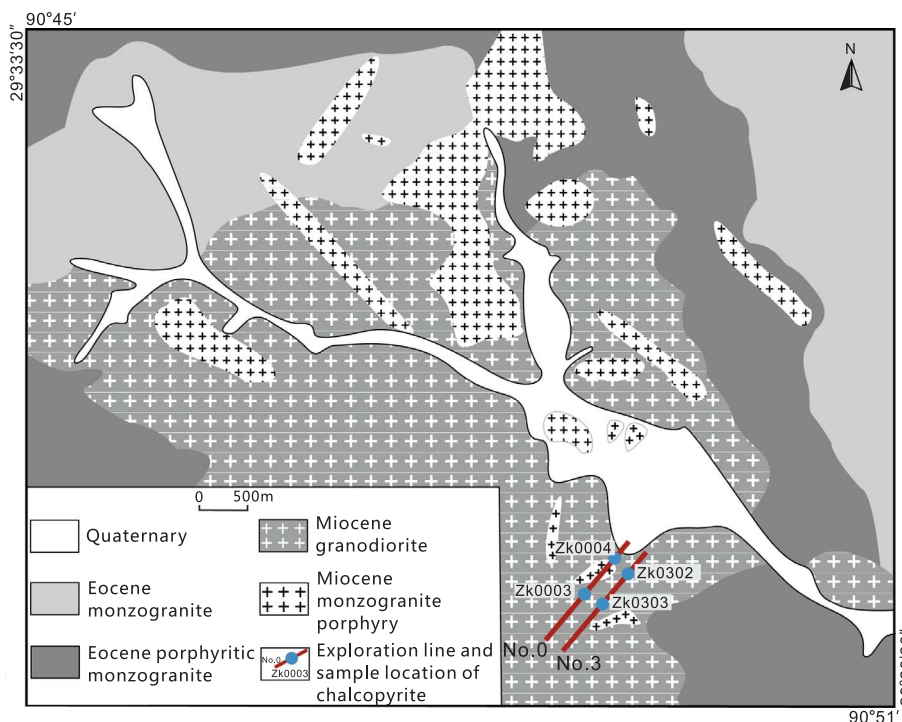


**Fig. 2.** Geological map of the Dabu porphyry Cu-Mo deposit (modified after Wu et al., 2014). The two red lines are exploration lines No. 0 and No. 3, respectively. Chalcopyrite samples were collected from four drill cores including ZK0004, ZK0003, ZK0303 and ZK0302. The blue circles denote the locations of the four drill cores.

### 3. Sample descriptions

Twenty-two chalcopyrite mineral separates were handpicked from drill core samples—including thirteen from ZK0004, four from ZK0302, two from ZK0303, and three from ZK0003—and were analyzed for Cu isotopic compositions. Because the average Cu grade in ZK0004 is greater than those of the other three drill cores, only samples in ZK0302, ZK0303 and ZK0003 that had sufficient chalcopyrite to handpick under a binocular microscope were collected for Cu isotope analysis. The locations of the sampled drill holes are shown in Fig. 2. Normally, the alteration zoning pattern of porphyry hydrothermal system changes from potassic at the core outward through phyllitic, argillic (quartz-kaolin-montmorillonite), to peripheral propylitic (epidote-calcite-chlorite) (Lowell and Gilbert, 1970). Potassic alteration is defined by formation of biotite in relatively mafic rocks and K-feldspar in more felsic rocks. Phyllitic alteration is commonly characterized by transformation of mafic minerals to chlorite, and plagioclase to fine-grained sericite (or illite) and quartz, and the altered rocks are pale-green, greenish-gray, or white (Sillitoe, 2010). The alteration and mineralization characteristics of selected samples from the Dabu deposit are shown in Figs. 3–5 and Table 1, and detailed descriptions are given below.

#### 3.1. ZK0004

The associated silicate alteration minerals in samples from drill hole ZK0004 form phyllitic, potassic, and argillic assemblages. Generally, the shallow (ZK0004-48, 68, 100) and deep (ZK0004-170, 201, 300, 472, 488, 494) portions of this drill hole are mainly dominated by phyllitic alteration, whereas the middle segment (ZK0004-130, 151, 178) contains potassic alteration. The phyllitic alteration assemblages are typically dominated by sericite, quartz, pyrite and chalcopyrite. The occurrence of sericite is variable; it forms alteration halos surrounding ore-bearing veins or veinlets (Fig. 3c), fills hairline cracks (Fig. 3d), and replaces feldspars (Fig. 3e). In the case of weak alteration, plagioclase phenocrysts show some sericite growth along hairline cracks or as alteration halos along the margin of veinlets, where the sericite is generally < 100 µm in size (Fig. 3d, e, k). Intense phyllitic alteration is

characterized by pervasive replacement of all silicate minerals except quartz by micro-grained sericite or alteration halos surrounding ore-bearing veins where sericite is mostly scaly to acicular and anhedral, with diameters mostly < 50 µm (Fig. 3 g, h, j, l). The main vein assemblages associated with phyllitic alteration include quartz-pyrite-chalcopyrite, quartz-molybdenite (Fig. 3c), quartz-pyrite, and quartz-chalcopyrite (Fig. 3 k, l) veins, which are planar in form with widths of 1–5 mm. Biotite-bearing veinlets include biotite-pyrite (Fig. 3f), quartz-chalcopyrite-biotite-pyrite, and quartz-biotite-molybdenite-chalcopyrite (Fig. 3i), which are irregular and continuous to discontinuous in form with variable widths of 0.2–5.0 mm, also show characteristics of phyllitic alteration dominated by well-developed sericitic halos (Fig. 3f, i). Pyrite and chalcopyrite grains are anhedral and irregular in shape, typically fractured, without other minerals filling the fractures. Argillic alteration is observed in the shallow sample from ZK0004-48, where it overprints earlier phyllitic alteration assemblages. This type of alteration is characterized by selective pervasive replacement of feldspar by clay minerals (Fig. 3b).

Potassic alteration consisting of K-feldspar alteration and biotite alteration is characterized by the formation of K-feldspar, biotite, and abundant quartz (Fig. 4). Vein- or veinlet-forming K-feldspar, including quartz-K-feldspar veinlets and quartz veins characterized by irregular to planar margins and the absence of sulfides, is the dominant style of K-feldspar alteration (Fig. 4a, c). K-feldspar in the veins typically shows intergrowths with quartz grains (Fig. 4b), or occurs discontinuously at the vein margins (Fig. 4c). Biotite alteration is characterized by the presence of abundant biotite, quartz, and minor K-feldspar, and occurs in two main modes: alteration halos along barren quartz veins (Fig. 4d), and as selective replacement of primary minerals such as biotite and feldspar (Fig. 4f). In the alteration halos, biotite is generally < 50 µm in size and has an irregular shape (Fig. 4e). Selective replacement resulted in biotite that is generally subhedral to euhedral in form and mainly < 0.1 mm in size (Fig. 4f). Potassic alteration is characterized by disseminated chalcopyrite in rocks or as clots in biotite halos (Fig. 4a).

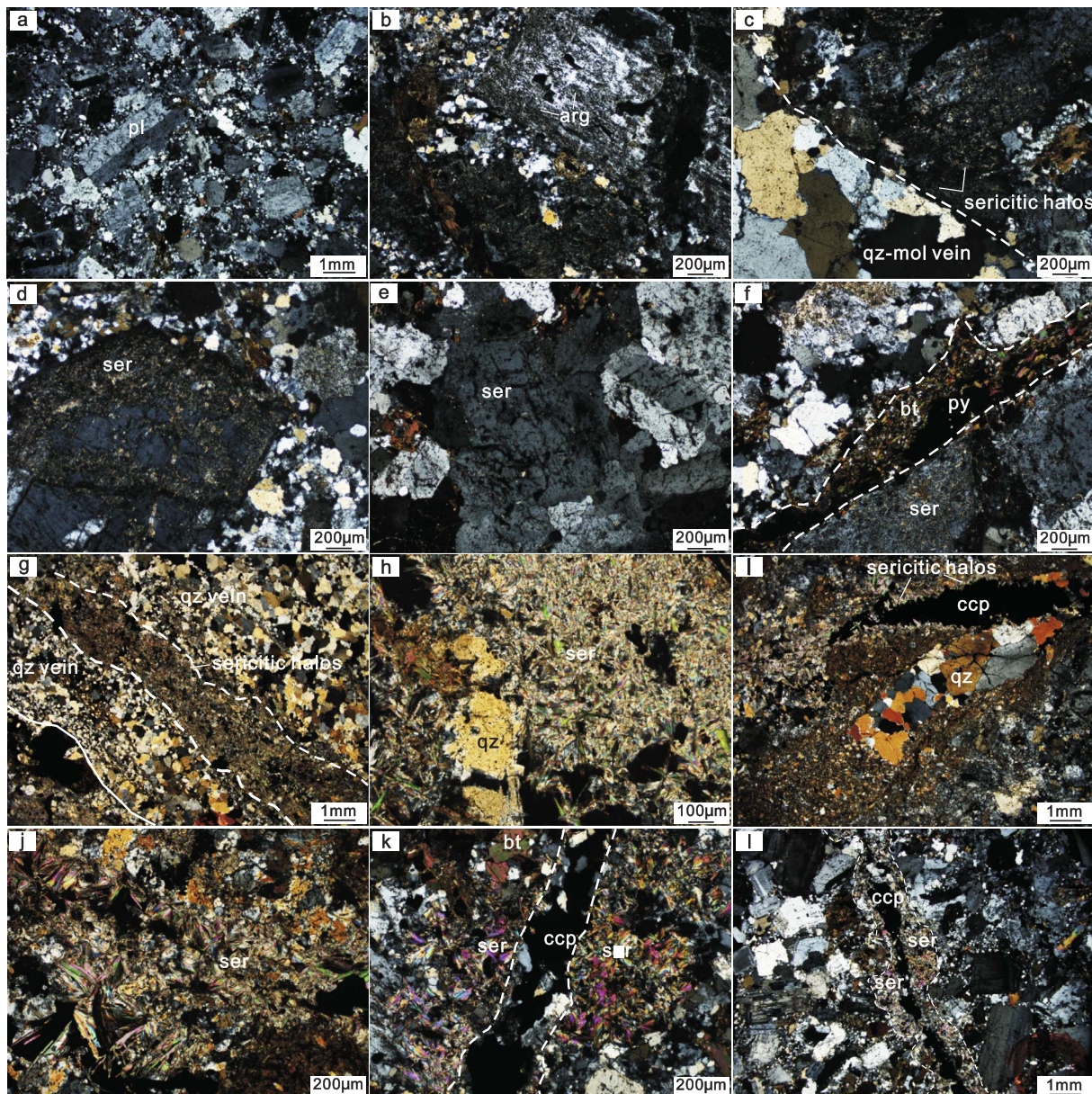


**Fig. 3.** Characteristics of alteration and mineralization assemblages in drill-core samples from ZK0004. (a) fresh monzogranite porphyry showing typical porphyritic texture (ZK0004-57). (b) Argillic alteration characterized by selective replacement of feldspar phenocrysts by clay minerals (ZK0004-48). (c) Coarse quartz-molybdenite vein surrounded by sericitic alteration halos (ZK0004-68). (d) Destructive alteration of a feldspar phenocryst into fine to medium-grained sericite (ZK0004-100). (e) Weak sericitic alteration (ZK0004-170). (f) biotite-pyrite veinlet showing sericitic alteration halos along its margins, and the biotite in this veinlet is generally anhedral with diameter < 50 µm (ZK0004-201). (g) Sericitic alteration halos around a quartz-pyrite-chalcopyrite ± molybdenite vein, (h) pervasive replacement of all silicate minerals except quartz by micro-grained sericite that is scaly-acicular and has distinct pleochroism (ZK0004-300). (i) quartz-biotite-chalcopyrite-pyrite veinlet showing the presence of sparsely disseminated chalcopyrite in the sericitic alteration halos, (j) sericitic alteration halos that are intensely developed around veinlets; the alteration sericite is mostly scaly-acicular with distinct pleochroism and generally less than 100 µm in diameter (ZK0004-472). (k) quartz-chalcopyrite veinlet showing sericitic alteration halos along its margins (ZK0004-488). (l) quartz-chalcopyrite veinlet showing intense phyllitic alteration halos characterized by nearly complete destruction of feldspars by micro-grained sericite that is scaly-acicular (ZK0004-494). Abbreviations: Qz quartz, pl plagioclase, ser sericite, arg argillic, ccp chalcopyrite, py pyrite, bt biotite, mol molybdenite.

### 3.2. ZK0302

Four samples from ZK0302 are dominated by phyllitic alteration, as evident from sericitic alteration halos along the margins of quartz-chalcopyrite veinlets, and selective pervasive mineral replacement of feldspar phenocrysts by white sericite and fine-grained quartz (Fig. 5a, b, d). The ore minerals include disseminated or minor chalcopyrite and pyrite filling along the fractures, as well as quartz-chalcopyrite veinlets (Fig. 5a, b, c).

### 3.3. ZK0303

Two samples from ZK0303 are characterized by weak phyllitic alteration, which are evident as sericitic alteration halos surrounding quartz-chalcopyrite veinlets and selective replacement of feldspar phenocrysts by fine-grained sericite (Fig. 5e, f). Mineralization includes quartz-chalcopyrite ± pyrite veinlets or disseminated chalcopyrite and pyrite fill along fractures or disseminated in rocks (Fig. 5e).

### 3.4. ZK0003

Three samples from ZK0003 are characterized by intense phyllitic

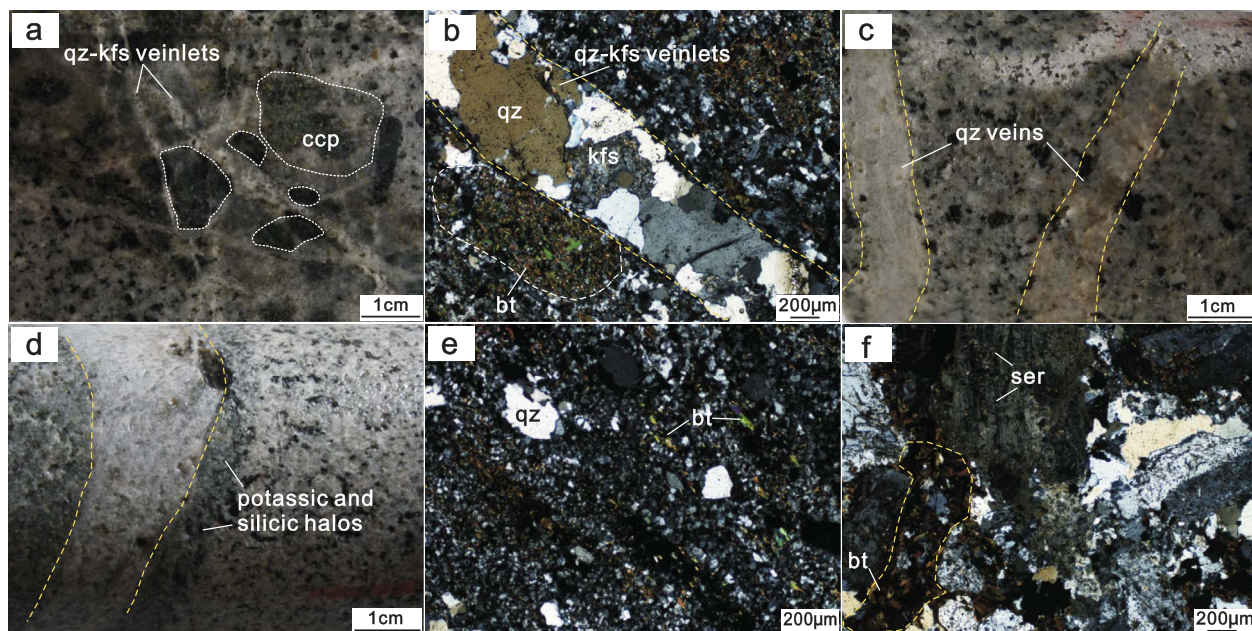


**Fig. 4.** Characteristics of potassic alteration in drill-core samples from ZK0004. (a) quartz- K-feldspar veinlets are locally surrounded by clusters of anhedral secondary biotite with diameters mostly < 0.1 mm and microcrystal quartz grains denoted by the white dotted line, in which the disseminated chalcopyrite occurs, (b) K-feldspar crystals within the veinlet show sericitic alteration (ZK0004-130). (c) Quartz veins are characterized by irregular to planar margins and the absence of sulfides, along which the potassic alteration halos occur that are dominated by micro-granular K-feldspar crystals, as well as disseminated potassic alteration in the whole rock (ZK0004-151). (d) Coarse quartz vein showing clear potassic and silicic alteration halos along its margins, (e) silicic alteration halos characterized by fine-grained quartz and linear-distributed long-lamina biotite, (f) potassic alteration characterized by clusters of anhedral biotite (ZK0004-178). Abbreviations: Qz quartz, kfs K-feldspar, ser sericite, bt biotite, ccp chalcopyrite.

alteration, as shown by nearly complete destruction of feldspars by fine-grained sericite and quartz (Fig. 5 g), as well as sericite locally replacing plagioclase (Fig. 5 i). Mineralization consists of disseminated chalcopyrite on fractures and minor star-shaped chalcopyrite aggregates among clusters of biotite (Fig. 5 h, i), as well as quartz-chalcopyrite veinlets.

#### 4. Analytical methods

The detailed procedures for sample digestion, column chemistry and instrumental analysis have been described in Liu et al. (2014a). Only a brief description is given below. The samples were crushed, and separates of chalcopyrite crystals were prepared with careful handpicking under a binocular microscope on the basis of size, clarity, color, and morphology to achieve a purity of 98%. A single grain of each of the twenty-two fresh chalcopyrite samples was selected for dissolution. The grains were dissolved in a 1:3 (v/v) mixed solution of double-distilled HNO<sub>3</sub> and HCl. After complete dissolution by heating and then evaporating to dryness at 80 °C, the samples were refluxed with concentrated HNO<sub>3</sub> and subsequently dried down at 80 °C. Then, 1 ml of 8 N HCl + 0.001% H<sub>2</sub>O<sub>2</sub> was added to the beaker and then heated to dryness at 80 °C, which was repeated three times to ensure that all cations were converted to chloride species prior to ion-exchange separation. The final materials of chalcopyrite samples were dissolved in 1 ml of 8 N HCl + 0.001% H<sub>2</sub>O<sub>2</sub> in preparation for ion-exchange separation. The separation of Cu was carried out by one-step column ion-exchange chromatography using strong anion resin AG-MP-1M. The Cu isotopic ratios were measured using a Thermo-Finnigan Neptune plus MC-ICP-MS at the Isotope Geochemistry Laboratory of the China University of Geosciences, Beijing. Sample-standard bracketing (SSB) method was used to correct for instrumental mass fractionation and drifting. Cu isotope ratios are reported in standard δ-notation in per mil relative to the standard reference material (SRM) NIST 976:  $\delta^{65}\text{Cu} = ((^{65}\text{Cu}/^{63}\text{Cu})_{\text{sample}}/(^{65}\text{Cu}/^{63}\text{Cu})_{\text{standard}} - 1) \times 1000$ . The long-term external reproducibility for  $\delta^{65}\text{Cu}$  measurements is better than ± 0.05‰ (2SD), as obtained from repeated analyses of natural samples and

synthetic solutions (Liu et al., 2014a, 2015).

#### 5. Results

The  $\delta^{65}\text{Cu}$  values of mineral separates of chalcopyrite from the Dabu deposit are summarized in Table 1. The overall Cu isotopic range from drill hole samples is from −1.48‰ to +1.12‰. In the No. 0 exploration line, mineral separates of chalcopyrite from ore-hosting monzon-granite porphyry in the drill hole ZK0003 show  $\delta^{65}\text{Cu}$  values of −0.37‰ to +0.08‰, whereas samples from drill hole ZK0004 exhibit a larger variation from −1.48‰ to +0.59‰ in  $\delta^{65}\text{Cu}$  values. In the No. 3 exploration line,  $\delta^{65}\text{Cu}$  values of chalcopyrite from the drill hole ZK0302 vary between +0.05‰ and +1.12‰, and two samples from drill hole ZK0303 have  $\delta^{65}\text{Cu}$  values of +0.06‰ and +0.15‰, respectively. In general, samples with potassic alteration have  $\delta^{65}\text{Cu}$  values varying from −1.48‰ to −0.95‰, whereas samples dominated by phyllitic alteration yield Cu isotopic compositions of −0.92‰ to +1.12‰. In addition, one sample with argillic alteration has  $\delta^{65}\text{Cu}$  values of −0.15‰, whereas another sample without alteration has  $\delta^{65}\text{Cu}$  values of +0.59‰.

#### 6. Discussion

##### 6.1. Cu isotope fractionation during hydrothermal evolution

Significant Cu isotope fractionation in ore forming system has been documented by previous Cu isotope studies of sulfide minerals in ore deposits (Fig. 6), and has been attributed to combinations of changes in pH, temperature, vapor-liquid partitioning, mineral-fluid reaction, as well as variable redox conditions (Graham et al., 2004; Rouxel et al., 2004; Mathur et al., 2005, 2013; Markl et al., 2006; Seo et al., 2007; Maher et al., 2011; Duan et al., 2015; Yao et al., 2016). For example, the Cu isotope compositions of chalcocite from sediment hosted vein-type deposit of Dikulushi in Congo become heavier toward the center of the orebody as the result of physicochemical changes to the mineralizing fluid, and the heavier Cu isotope compositions of chalcocite

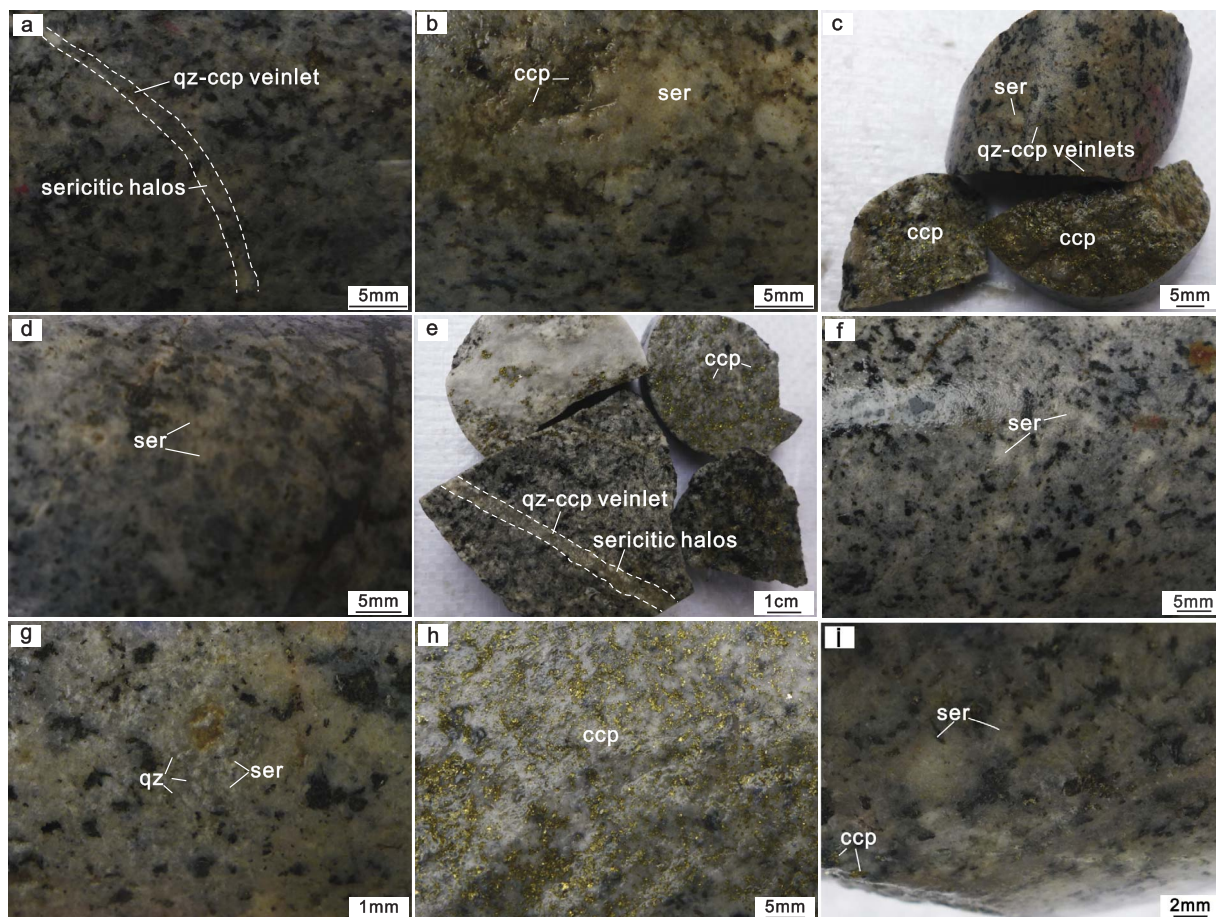


**Fig. 5.** Characteristics of alteration and mineralization assemblages in drill-core samples from ZK0302, ZK0303 and ZK0003. (a) quartz-chalcopyrite veinlet showing sericitic alteration halos along its margins (ZK0302-63). (b) Chalcopyrite fill along fractures, close to which phyllitic alteration characterized by destruction of feldspar phenocrysts into fine-grained sericite and quartz is developed (ZK0302-119). (c) Chalcopyrite in open fractures and quartz-chalcopyrite veinlets, together with sericitic alteration dominated by sericite locally replacing plagioclase (ZK0302-334). (d) White sericitic alteration (ZK0302-483). (e) Sparsely disseminated chalcopyrite and pyrite, and quartz-chalcopyrite veinlet surrounded by white sericitic alteration halos (ZK0303-206). (f) Weak sericitic alteration dominated by selective replacement of feldspar phenocrysts by fine-grained sericite (ZK0303-238). (g) Phyllitic alteration characterized by nearly complete destruction of feldspars by fine-grained sericite and quartz (ZK0003-263). (h) Disseminated chalcopyrite on fractures associated with phyllitic alteration (ZK0003-350). (i) Minor star-like distributed chalcopyrite, and phyllitic alteration characterized by sericite locally replacing feldspars (ZK0003-373). Abbreviations: Qz quartz, ser sericite, arg argillic, CCP chalcopyrite, py pyrite.

from Cu-Ag mineralization was interpreted as the partial remobilization of early Cu-Pb-Zn-Fe mineralization in an oxidizing environment (Haest et al., 2009). A genetic correlation between depositional temperature and large isotopic variations of chalcopyrite has been inferred in a sediment hosted vein-type deposit of Jinman in China, with higher temperature Cu sulfides having higher  $\delta^{65}\text{Cu}$  values (Jiang et al., 2002). The chalcopyrite samples from sea floor hydrothermal deposits show a larger variation in  $\delta^{65}\text{Cu}$  values from  $-4.82\text{\textperthousand}$  to  $+11.71\text{\textperthousand}$ , which can be explained by complex processes in sea floor hydrothermal system involving fluid mixing, circulation and oxidation of seawater, as well as alteration and remobilization of sulfide minerals (Zhu et al., 2000; Rouxel et al., 2004). Chalcopyrite from volcanic-associated massive sulfide (VMS) deposits ( $-0.62\text{\textperthousand}$  to  $+0.34\text{\textperthousand}$ ; Mason et al., 2005; Housh and Çiftçi, 2008; Ikehata et al., 2011) and sulfide minerals from mafic-ultramafic magmas associated Cu-Ni-PGE (platinum-group elements) deposits ( $-2.3\text{\textperthousand}$  to  $+1.0\text{\textperthousand}$ ; Malitch et al., 2014; Zhao et al., 2017) have low and in most cases negative  $\delta^{65}\text{Cu}$  values. A similar pattern is observed in sediment-hosted stratiform copper (SSC) deposits ( $-3.77\text{\textperthousand}$  to  $+0.65\text{\textperthousand}$ ; Asael et al., 2007, 2009, 2012) and vein-type deposits ( $-2.3\text{\textperthousand}$ – $0\text{\textperthousand}$ ; Haest et al., 2009). At the Bingham porphyry Cu deposit, samples located furthest from the source intrusion are more enriched in  $^{65}\text{Cu}$  relative to samples closest to the center of hydrothermal system, and Cu isotope values gradually increase outward from the porphyry intrusion (Dendas, 2011). All of these studies indicate the

variation in copper isotope fractionation exists and Cu isotopes can be used as an exploration tool to vector fluid flow pathways, and identify multiple mineralization or remobilization events (Graham et al., 2004; Maher and Larson, 2007; Haest et al., 2009; Li et al., 2010; Braxton and Mathur, 2011; Dendas, 2011; Mathur et al., 2013).

For porphyry Cu deposits, the  $\delta^{65}\text{Cu}$  values of hypogene copper-rich minerals precipitated at high temperature cluster between  $-1\text{\textperthousand}$  and  $+1\text{\textperthousand}$  (Fig. 6; Mathur et al., 2009). The  $\delta^{65}\text{Cu}$  values of chalcopyrite in the Dabu deposit show a variation of up to  $2.60\text{\textperthousand}$ , slightly larger than the main cluster observed in other porphyry systems. The chalcopyrite samples from four drill holes in the Dabu deposit reveal a gradually increasing trend of Cu isotope values from  $-1.48\text{\textperthousand}$  at a depth of 130 m to  $1.12\text{\textperthousand}$  at a depth of 483 m, no matter the sampling depth of single drill hole or converted elevation is used when plotting (Fig. 7). At the shallow levels, the  $\delta^{65}\text{Cu}$  values of the chalcopyrite increase from  $-1.48\text{\textperthousand}$  at a depth of 130 m to  $0.59\text{\textperthousand}$  at a depth of 57 m (Fig. 7). This suggests that Cu may have been fractionated during the hydrothermal evolution of the porphyry deposit. These variation trends differ from those observed in the Pebble porphyry Cu-Au-Mo deposit, where a systematic increase in  $\delta^{65}\text{Cu}$  values from deeper to shallower levels of hypogene mineralization has been reported (Mathur et al., 2013).

To further evaluate the behaviors of Cu isotopes at high temperature during hydrothermal processes, some important issues should first be addressed, including the partitioning of Cu isotopes between

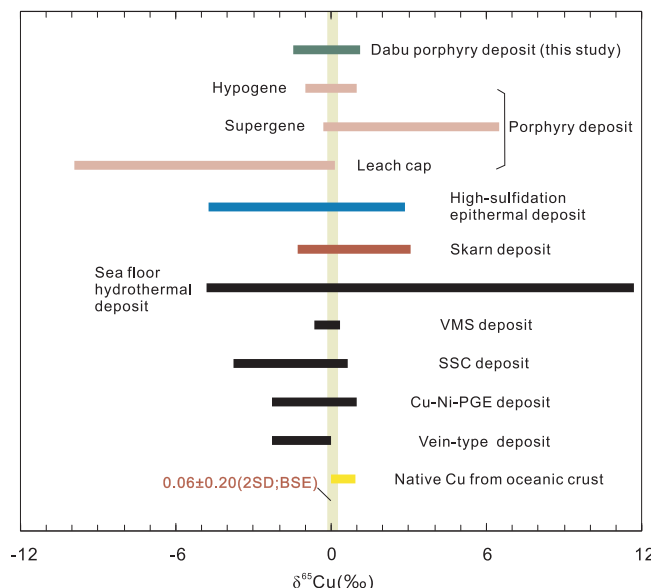
**Table 1**

Copper isotope data and descriptions of samples from four drill holes in the Dabu deposit, southern Tibet.

Hole ID	Depth (m)	Elevation (m)	Alteration Type	Alteration Mineral Assemblages	Occurrence of Ore Mineral	$\delta^{65}\text{Cu}$ (‰)	$\pm 2\text{SD}$ (‰)	N <sup>a</sup>
ZK0003	263	4337	Phyllitic	Qz, Ser	Disseminated CCP filling along the fracture	-0.37	0.05	3
ZK0003	350	4250	Phyllitic	Qz, Ser	Disseminated CCP and minor py filling along the fracture	0.08	0.05	3
ZK0003	373	4227	Phyllitic	Qz, Ser	Minor star-like distributed CCP in cluster of biotite	-0.10	0.08	3
ZK0302	63	4277	Phyllitic	Ser	Qz-CCP veinlet, and fractured CCP and py	0.05	0.05	3
ZK0302	119	4221	Phyllitic	Ser and minor Qz	Sparingly disseminated CCP and py on the fracture	0.09	0.05	3
ZK0302	334	4006	Phyllitic	Ser	Qz-CCP veinlets and disseminated CCP filling along the fracture	0.42	0.06	3
ZK0302	483	3857	Phyllitic	Ser	Disseminated CCP and minor py filling along the fracture	1.12	0.05	3
ZK0303	206	4214	Phyllitic	Ser	Qz-CCP-py veinlet, sparsely disseminated CCP and py in rocks	0.06	0.05	3
ZK0303	238	4182	Phyllitic	Ser	Sparingly disseminated CCP and py in rocks	0.15	0.05	3
ZK0004	48	4382	Phyllitic, Argillic	Clay minerals, Ep and minor Ser	Qz-py veinlets and minor star-like distributed CCP in rocks	-0.15	0.16	3
ZK0004	57	4373	No	No	Qz-mol veinlet, sparsely disseminated py filling along the fracture and minor star-like distributed CCP in rocks	0.59	0.05	3
ZK0004	68	4362	Phyllitic	Ser	Qz-mol vein and qz-py-CCP veinlets	-0.92	0.05	3
ZK0004	100	4330	Phyllitic	Ser	Disseminated CCP filling along the fracture and qz-CCP vein	-0.60	0.05	3
ZK0004	130	4300	Potassic, Silicic	Qz, Kfs, Bt	Locally disseminated CCP in rocks	-1.48	0.05	3
ZK0004	151	4279	Potassic	Qz, Kfs, Bt	Qz-kfs-CCP ± py veinlets	-1.12	0.05	3
ZK0004	170	4260	Phyllitic	Qz, Ser	Minor star-like distributed chalcopyrite in rocks	-0.23	0.05	3
ZK0004	178	4252	Potassic	Qz, Kfs, Bt and minor Ser	Qz-kfs-bt-CCP vein and disseminated CCP in rocks	-0.95	0.08	3
ZK0004	201	4229	Phyllitic	Qz, Ser, Bt	Bt-py veinlet and qz-py-mol ± CCP vein	0.17	0.06	3
ZK0004	300	4130	Phyllitic	Qz, Ser	Qz-py-CCP ± mol vein	0.15	0.06	3
ZK0004	472	3958	Phyllitic	Qz, Ser, Bt	Qz-py-mol vein and qz-bt-CCP-py veinlet	0.21	0.05	3
ZK0004	488	3942	Phyllitic	Qz, Ser	Qz-CCP-py-mol veinlets and sparsely disseminated CCP in rocks	0.24	0.05	3
ZK0004	494	3936	Phyllitic	Qz, Ser	Qz-CCP-py veinlets	0.32	0.08	3

2SD 2 times the standard deviation of the population of n repeat measurements of a sample solution.

Abbreviations: Qz quartz, kfs K-feldspar, ser sericite, CCP chalcopyrite, py pyrite, bt biotite, mol molybdenite, Ep epidote.

<sup>a</sup> N represents the number of repeat measurements of the same purification solution by MC-ICP-MS.

**Fig. 6.** Diagram showing variation in  $\delta^{65}\text{Cu}$  values of chalcopyrite in the Dabu deposit, compared to previous studies on copper-rich minerals from porphyry deposit (Mathur et al., 2009), high-sulfidation epithermal deposit (Duan et al., 2015; Wu et al., 2017b), skarn deposit (Maher and Larson, 2007; Wang et al., 2017), sea floor hydrothermal deposit (Zhu et al., 2000; Rouxel et al., 2004), volcanic-associated massive sulfide (VMS) deposits (Mason et al., 2005; Housh and Çiftçi, 2008; Ikehata et al., 2011), Cu-Ni deposit (Malitch et al., 2014; Zhao et al., 2017), sediment-hosted stratiform copper (SSC) deposit (Asael et al., 2007, 2009, 2012), vein-type deposit (Haest et al., 2009), as well as native Cu from oceanic crust (Dekov et al., 2013). The light gray bar represents the  $\delta^{65}\text{Cu}$  range of the bulk silicate Earth (BSE) ( $-0.14\text{‰}$  to  $+0.26\text{‰}$ ; Liu et al., 2015).

hydrothermal fluids and precipitating Cu sulfides, and the speciation of Cu in porphyry hydrothermal systems. Previous studies suggested that chloride and bisulfide complexes such as  $\text{CuCl}_2^-$  and  $\text{Cu}(\text{HS})_2^-$  are the

dominant species of Cu in the fluid under typical porphyry P-T conditions (Mountain and Seward, 1999, 2003; Pokrovski et al., 2008), indicating the majority of copper in hydrothermal fluid is +1, consistent with the measured valence state of copper in chalcopyrite using X-ray techniques (Pearce et al., 2006). To date, no experimental Cu isotope fractionation factors between sulfides and hydrothermal solutions have been published, with the exception of two theoretical studies (Seo et al., 2007; Maher et al., 2011). For example, a study of chalcopyrite solubility in chloride-bearing aqueous fluids by Maher et al. (2011) show that  $^{65}\text{Cu}$  isotope fractionation between hydrothermal fluids and sulfides is small ( $\leq 1\text{‰}$ ) at temperatures of  $250\text{ }^\circ\text{C}$  and  $300\text{ }^\circ\text{C}$ . Thus, redox reactions due to change of valence states during hydrothermal evolution, and Cu isotope fractionation between hydrothermal fluids and precipitated sulfides, are unlikely to cause the Dabu Cu isotope variation.

Based on the detailed observation of alteration and mineralization of analyzed samples in the Dabu deposit (Table 1; Figs. 3–5), we found that the patterns of the Cu isotope ratios vary with depth and the type of silicate alteration present (Figs. 7–9). In general, the Cu isotope values show a pattern where heavier values characterized by both deep and shallow samples corresponding to areas of lower temperature alteration assemblages such as phyllitic and argillic alteration. In comparison, the lighter values characterize samples associated with high temperature potassic alteration. The Cu isotope values display a gradually increasing trend from  $-1.48\text{‰}$  to  $0.59\text{‰}$  with a decrease in depth, as well as the change of alteration assemblages from potassic, phyllitic, through argillic alteration to relatively fresh (Figs. 7 and 9). Similarly, the  $\delta^{65}\text{Cu}$  values of the chalcopyrite show a gradual increasing trend from  $-1.48\text{‰}$  to  $1.12\text{‰}$  with the increasing of drilling depth, as well as the change of alteration from potassic to phyllitic (Figs. 7 and 9). Variability in the  $\delta^{65}\text{Cu}$  values observed at the Dabu deposit was similar to those of the Pebble porphyry Cu-Au-Mo Deposit in Alaska, both of which show a correlation with different silicate alteration assemblages formed at different temperatures (Mathur et al., 2013). Therefore, a Rayleigh precipitation process, coupled with the decrease in temperature, is a

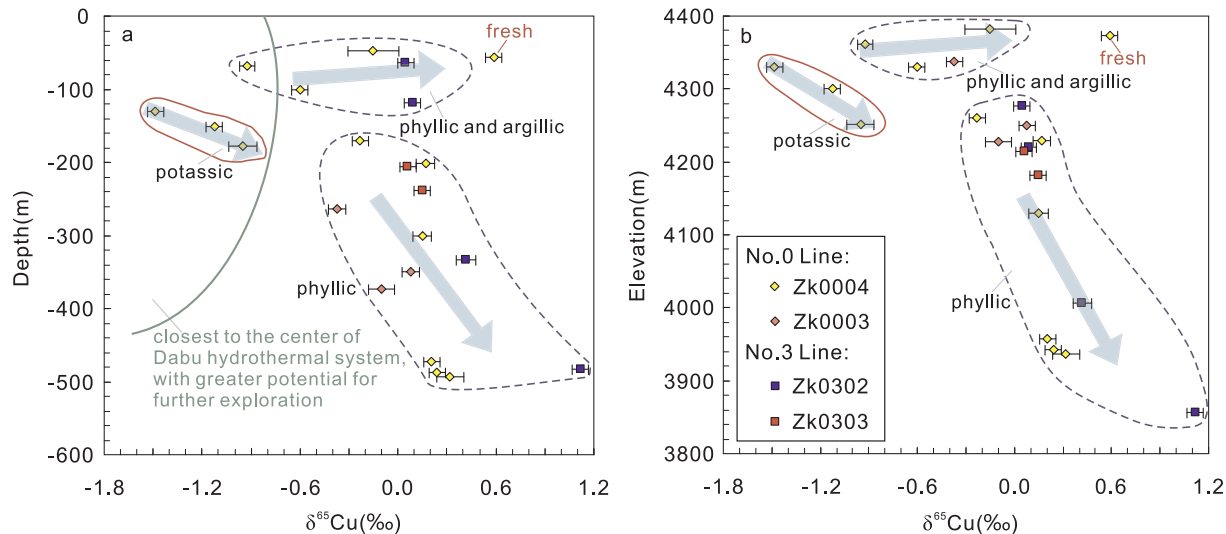


**Fig. 7.** Variation of Cu isotope compositions of chalcopyrite from drill hole ZK0003, ZK0004, ZK0302 and ZK0303 with depth and elevation, indicating the genetic link between Cu isotope variation and silicate alteration assemblages formed at different temperatures. The arrows denote the hydrothermal fluid pathways.

possible mechanism for explaining the large variation of  $\delta^{65}\text{Cu}$  (up to 2.6‰) at Dabu deposit. Due to the uncertainty of Cu isotope fractionation factors between fluid and sulfide minerals, as well as the complicated physical and chemical conditions for hydrothermal systems, it is hard to simulate the Rayleigh precipitation process adequately. [Seo et al. \(2007\)](#) used Density Function Transfer theory to calculate the reduced partition function ratios of different copper solution complexes, which predicted fractionation of copper isotopes at high temperatures (approximately 0.5‰ fractionation at > 300 °C) during cooling of hydrothermal fluids and precipitation of Cu. As a preliminary study, [Li et al. \(2010\)](#) have simulated the  $\delta^{65}\text{Cu}$  of precipitated Cu from a theoretical solution with a starting  $\delta^{65}\text{Cu}$  value of 0.2‰ and assuming

temperature-based fractionation factors of  $\delta^{65}\text{Cu}_{\text{solution-sulfide}} = -0.6$  to +0.6; modeling shows a variation of Cu isotope values as temperature decreases from 390 °C to 320 °C. As shown in [Fig. 10](#), the magnitude of Cu isotope fractionation ( $\delta^{65}\text{Cu}$  is approximately 2.6‰) of chalcopyrite minerals precipitated at Dabu can be explained and predicted when assuming a fluid–sulfide isotopic fractionation factor of 0.6, according to the model of a Rayleigh-type precipitation process proposed by [Li et al. \(2010\)](#).

According to the Rayleigh distillation model of vapor–liquid partitioning of Cu and Mo isotopes during cooling of hydrothermal solutions, coupled with fluid inclusions and H–O data of quartz, [Yao et al. \(2016\)](#) demonstrated that vapor–liquid fractionation could be the cause

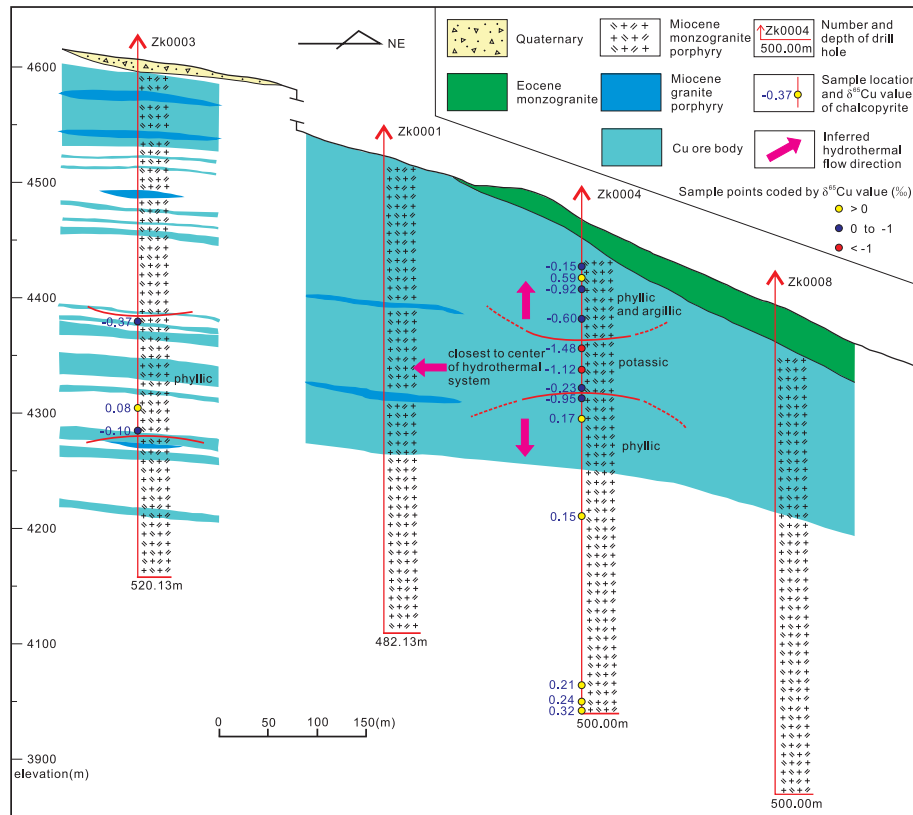


**Fig. 8.** Simplified geologic section of the No. 0 exploration line in the Dabu Cu-Mo deposit, showing spatial relationships among intrusions, silicate alteration assemblages, and Cu isotopic variation of chalcopyrite (modified from the collected map from Tibet Institute of Geological Survey in 2011).

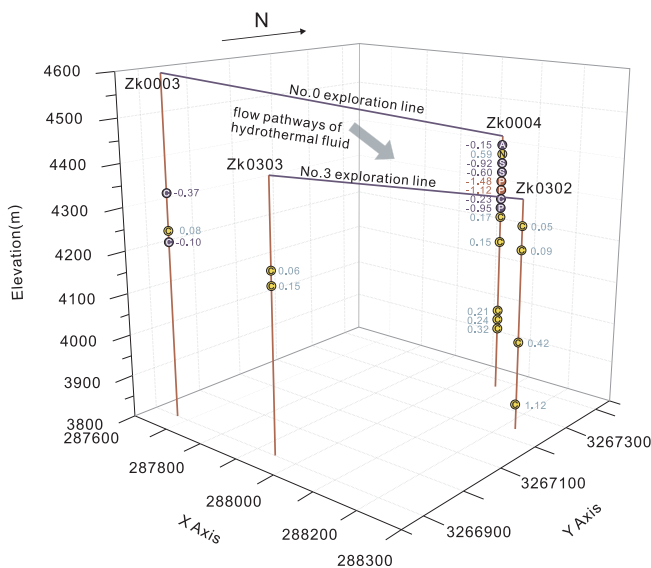


**Fig. 9.** Three-dimensional plot of  $\delta^{65}\text{Cu}$  values, alteration types and exact locations of samples from four drill holes in the Dabu deposit. Abbreviations: P-potassic alteration, C-phyllitic alteration, A-argillic alteration, N-no alteration.

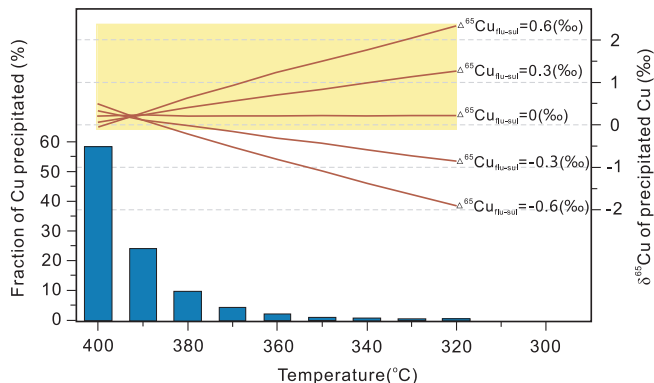


**Fig. 10.** Model of Cu isotopic compositions of precipitated Cu solely by a Rayleigh-type fractionation process. Full details of the modeling are provided in Li et al. (2010). The yellow area represents the magnitude of Cu isotope fractionation ( $\delta^{65}\text{Cu}$  is approximately 2.6‰) of chalcopyrite minerals precipitated at Dabu deposit.

for the isotopic values measured in the Dahutang W-Cu-Mo ore field, China. For natural high-temperature porphyry systems, hydrothermal experiments and fluid inclusion studies revealed that Cu is preferentially partitioned into the vapor phase rather than the brine as a function of water fugacity and S (Heinrich et al., 1999; Williams-Jones and Heinrich, 2005; Simon et al., 2006; Pokrovski et al., 2008; Seo et al., 2009). Thus, it is likely that the vapor transport of Cu is the most likely agent, although post-trapping diffusion processes could also result in the enrichment of Cu into vapor-rich fluid inclusions (Lerchbaumer and Audébat, 2012). Otherwise, the quantum chemical calculations of equilibrium Cu isotope fractionation (Seo et al., 2007) reveal that Cu in vapor species ( $\text{CuCl}(\text{H}_2\text{O})$  and  $\text{Cu}_3\text{Cl}_3$ ) are significantly enriched in heavy Cu isotope ( $^{65}\text{Cu}$ ). However, the quantum calculations do not take into account the possible kinetic enrichment of light Cu isotope ( $^{63}\text{Cu}$ ) in the vapor, and experimental studies indicate preferential fractionation of light Cu isotope ( $^{63}\text{Cu}$ ) into the vapor, which is controlled by pH and salinity (Maher et al., 2011), we thus prefer that vapor is more likely enriched in  $^{63}\text{Cu}$  relative to  $^{65}\text{Cu}$  (Cooke et al., 2014). In the Dabu study, we therefore propose that the compositions of the initial Cu-bearing fluid was dominated by a vapor-phase that was enriched in  $^{63}\text{Cu}$  after phase separation or fluid boiling, which is a common phenomenon in porphyry deposit (Sillitoe, 2010). When fluids

flow to shallow or deep portions, accompanied by decreasing temperature during cooling, the Cu isotope values of precipitated sulfide minerals should gradually become isotopically heavier. To better constrain the metal precipitation-transportation ore-forming process, further investigations on the fractionation behavior of copper isotopes at high temperature magmatic-hydrothermal conditions are certainly needed.

## 6.2. Implications for mineral exploration

In a study of Cañariaco Norte porphyry copper deposit in northern Peru, Mathur et al. (2012) found that the majority of measured Cu sulfide minerals have a typical hypogene Cu isotope composition of  $0.18 \pm 0.38\text{\textperthousand}$ , with no significant supergene enrichment existing beneath the leached cap. According to mass balance constraints, the nonexistence of an enriched  $^{65}\text{Cu}$  reservoir suggested the presence of an undiscovered lateral/exotic Cu occurrence that enriched  $^{65}\text{Cu}$  that remained in solution during weathering. Similarly, Duan et al. (2015) made a systematic investigation of the Cu isotope compositions of Cu sulfide minerals from four drill holes in the Tiegelongnan high-sulfidation copper deposit, Tibet. They found a large Cu isotopic range of samples from two drill holes (up to 7.8‰) reflecting the low-temperature supergene processes, whereas two other drill holes from this deposit show the absence of isotopically heavy or light zones. Mass balance considerations suggest the missing zones are most likely hidden mineralized targets at depth in a porphyry copper system (Duan et al., 2015). Furthermore, in a study of Pebble porphyry Cu-Au-Mo deposit in Alaska, Mathur et al. (2013) used the correlation between  $\delta^{65}\text{Cu}$  values and silicate alteration assemblages to propose that Cu isotope values could be used to vector towards mineralized rocks. These examples demonstrated the possible application of Cu isotope variations to guide mineral exploration in a single closed mineralized system.

In this study of Dabu porphyry Cu-Mo deposit, as discussed above, the  $\delta^{65}\text{Cu}$  values in samples dominated by potassic alteration are isotopically lighter, whereas samples showing phyllitic and argillic alteration types formed during a later and lower temperature hydrothermal event are isotopically heavier (Figs. 7–9). In addition, the Cu isotope values of chalcopyrite from the No. 3 exploration line are higher than those of samples from the No. 0 exploration line at the same depth (Figs. 7 and 9). We therefore infer that chalcopyrite that precipitated early during potassic alteration formed at higher temperatures would be depleted in  $^{65}\text{Cu}$ , and would indicate the center of the hydrothermal system (Fig. 8). The hydrothermal fluid pathway should be from the No. 0 to the No. 3 exploration line (Fig. 9), and from the middle segment to both shallow and deep portions as marked in Fig. 8. Thus, the northwest side of No. 0 exploration line has greater potential for hosting extensions of mineralization, where the center of the Dabu high temperature system is located.

## 7. Conclusions

The Cu isotope values of chalcopyrite handpicked from four drill hole samples of Dabu deposit show a large variation of up to 2.6‰; these chalcopyrite samples were probably affected by a Rayleigh precipitation process during hydrothermal evolution with decreasing temperature. The data from Dabu deposit show that low Cu isotope values characterize samples closest to the center of hydrothermal system, which is dominated by potassic alteration, formed at high temperature. Relatively enriched Cu isotope values characterize samples peripheral to the center of hydrothermal system, which is dominated by phyllitic and argillic alteration, and formed at relatively low temperature. Based on the genetic link between Cu isotope variation and silicate alteration assemblages formed at different temperatures, we propose that hydrothermal fluid pathways should be from the No. 0 to the No. 3 exploration line, and from the middle segment to both shallow and deep portions. The pattern of Cu isotope variations in

conjunction with alteration mineralogy could provide potential insight into high temperature copper ore forming systems, constraining hydrothermal flow directions, and guiding mineral exploration.

## Acknowledgments

We are grateful to Associate Editor Jeffrey Mauk, Profs. Ryan Mathur, and two anonymous reviewers for their constructive comments and suggestions, which have significantly improved this manuscript. Funding for this project was jointly granted by the Commonwealth Project from the Ministry of Land and Resources, China (201511015), Changjiang Scholars and Innovative Research Team in University (IRT14R54, IRT1083), the China Geological Survey (DD20160027-2), and Fundamental Research Funds for the Central Universities (2-9-2017-201). Yiwen Lv, Dandan Li, and Zezhou Wang are greatly appreciated for their help in the lab.

## References

- Asael, D., Matthews, A., Bar-Matthews, M., Halicz, L., 2007. Copper isotope fractionation in sedimentary copper mineralization (Timna Valley, Israel). *Chem. Geol.* 243, 238–254.
- Asael, D., Matthews, A., Oszczepalski, S., Bar-Matthews, M., Halicz, L., 2009. Fluid speciation controls of low temperature copper isotope fractionation applied to the Kupferschiefer and Timna ore deposits. *Chem. Geol.* 262, 147–158.
- Asael, D., Matthews, A., Bar-Matthews, M., Harlavani, Y., Segal, I., 2012. Tracking redox controls and sources of sedimentary mineralization using copper and lead isotopes. *Chem. Geol.* 310–311, 23–35.
- Ben Othman, D., Luck, J., Bodinier, J., Arndt, N., Albarede, F., 2006. Cu–Zn isotopic variations in the Earth's mantle. *Geochim. Cosmochim. Acta* 70, A46.
- Bigalke, M., Weyer, S., Kobza, J., Wilcke, W., 2010. Stable Cu and Zn isotope ratios as tracers of sources and transport of Cu and Zn in contaminated soil. *Geochim. Cosmochim. Acta* 74, 6801–6813.
- Braxton, D., Mathur, R., 2011. Exploration applications of copper isotopes in the supergene environment: a case study of the Bayugo porphyry copper-gold Deposit, southern Philippines. *Econ. Geol.* 106, 1447–1463.
- Chung, S.L., Chu, M.F., Ji, J., O'Reilly, S.Y., Pearson, N.J., Liu, D., Lee, T.Y., Lo, C.H., 2009. The nature and timing of crustal thickening in Southern Tibet: Geochemical and zircon Hf isotopic constraints from postcollisional adakites. *Tectonophysics* 477, 36–48.
- Cooke, D.R., Hollings, P., Wilkinson, J.J., Tosdal, R.M., 2014. Geochemistry of porphyry deposits. In: Turekian, K.K., Holland, H.D. (Eds.), *Treatise on Geochemistry*, second ed. Elsevier, Oxford, pp. 357–381.
- Dekov, V.M., Rouxel, O., Asael, D., Hälenius, U., Munnik, F., 2013. Native Cu from the oceanic crust: isotopic insights into native metal origin. *Chem. Geol.* 359, 136–149.
- Dendas, M., 2011. Copper Isotope Tracers of Fluid Flow at Bingham Canyon Mine. The University of Arizona, Master, Utah.
- Duan, J., Tang, J., Li, Y., Liu, S.A., Wang, Q., Yang, C., Wang, Y., 2015. Copper isotopic signature of the Tiegelonglong high-sulfidation copper deposit, Tibet: implications for its origin and mineral exploration. *Mineral. Deposita* 51, 591–602.
- El Azzi, D., Viers, J., Guiresse, M., Probst, A., Aubert, D., Caparros, J., Charles, F., Guizien, K., Probst, J.L., 2013. Origin and fate of copper in a small Mediterranean vineyard catchment: new insights from combined chemical extraction and delta<sup>65</sup>Cu isotopic composition. *Sci. Total Environ.* 463–464, 91–101.
- Graham, S., Pearson, N., Jackson, S., Griffin, W., O'Reilly, S.Y., 2004. Tracing Cu and Fe from source to porphyry: in situ determination of Cu and Fe isotope ratios in sulfides from the Grasberg Cu–Au deposit. *Chem. Geol.* 207, 147–169.
- Haest, M., Muchez, P., Petit, J.C., Vanhaecke, F., 2009. Cu isotope ratio variations in the Dikulushi Cu–Ag deposit, DRC: of primary origin or induced by supergene reworking? *Econ. Geol.* 104, 1055–1064.
- Heinrich, C., Günther, D., Audétat, A., Ulrich, T., Frischknecht, R., 1999. Metal fractionation between magmatic brine and vapor, determined by microanalysis of fluid inclusions. *Geology* 27, 755–758.
- Hou, Z., Zhang, H., Pan, X., Yang, Z., 2011. Porphyry Cu (–Mo–Au) deposits related to melting of thickened mafic lower crust: Examples from the eastern *Tethyan metallogenetic domain*. *Ore Geol. Rev.* 39, 21–45.
- Housh, T., Çiftçi, E., 2008. Cu isotope geochemistry of volcanogenic massive sulphide deposits of the eastern Pontides, Turkey, IOP Conference Series: Earth and Environmental Science. IOP Publishing, p. 012025.
- Huang, J., Liu, S.A., Worner, G., Yu, H.M., Xiao, Y.L., 2016. Copper isotope behavior during extreme magma differentiation and degassing: a case study on Laacher See phonolitic tephra (East Eifel, Germany). *Contrib. Mineral. Petrol.* 171. <http://dx.doi.org/10.1007/s00410-016-1282-4>.
- Ikehata, K., Notsu, K., Hirata, T., 2011. Copper isotope characteristics of copper-rich minerals from besshi-type volcanogenic massive sulfide deposits, Japan, determined using a femtosecond LA-ICP-MS. *Econ. Geol.* 106, 307–316.
- Ji, W.Q., Wu, F.Y., Chung, S.L., Li, J.X., Liu, C.Z., 2009. Zircon U–Pb geochronology and Hf isotopic constraints on petrogenesis of the Gangdese batholith, southern Tibet. *Chem. Geol.* 262, 229–245.
- Jiang, S., Woodhead, J., Yu, J., Pan, J., Liao, Q., Wu, N., 2002. A reconnaissance of Cu isotopic compositions of hydrothermal vein-type copper deposit Jinman, Yunnan, China. *Chin. Sci. Bull.* 47, 249–251.
- Jouvin, D., Weiss, D.J., Mason, T.F., Bravin, M.N., Louvat, P., Zhao, F., Ferec, F., Hinsinger, P., Benedetti, M.F., 2012. Stable isotopes of Cu and Zn in higher plants: evidence for Cu reduction at the root surface and two conceptual models for isotopic fractionation processes. *Environ. Sci. Technol.* 46, 2652–2660.
- Larson, P.B., Maher, K., Ramos, F.C., Chang, Z., Gaspar, M., Meinert, L.D., 2003. Copper isotope ratios in magmatic and hydrothermal ore-forming environments. *Chem. Geol.* 201, 337–350.
- Lee, H.Y., Chung, S.L., Ji, J., Qian, Q., Gallet, S., Lo, C.H., Lee, T.Y., Zhang, Q., 2012. Geochemical and Sr–Nd isotopic constraints on the genesis of the Cenozoic Linzizong volcanic successions, southern Tibet. *J. Asian Earth Sci.* 53, 96–114.
- Lerchbaumer, L., Audétat, A., 2012. High Cu concentrations in vapor-type fluid inclusions: an artifact? *Geochim. Cosmochim. Acta* 88, 255–274.
- Li, W., Jackson, S.E., Pearson, N.J., Alard, O., Chappell, B.W., 2009. The Cu isotopic signature of granites from the Lachlan Fold Belt, SE Australia. *Chem. Geol.* 258, 38–49.
- Li, W., Jackson, S.E., Pearson, N.J., Graham, S., 2010. Copper isotopic zonation in the Northparkes porphyry Cu–Au deposit, SE Australia. *Geochim. Cosmochim. Acta* 74, 4078–4096.
- Liu, S.A., Li, D., Li, S., Teng, F.Z., Ke, S., He, Y., Lu, Y., 2014a. High-precision copper and iron isotope analysis of igneous rock standards by MC-ICP-MS. *J. Anal. At. Spectrom.* 29, 122–133.
- Liu, S.A., Teng, F.Z., Li, S.G., Wei, G.J., Ma, J.L., Li, D.D., 2014b. Copper and iron isotope fractionation during weathering and pedogenesis: insights from saprolite profiles. *Geochim. Cosmochim. Acta* 146, 59–75.
- Liu, S.A., Huang, J., Liu, J., Wörner, G., Yang, W., Tang, Y.J., Chen, Y., Tang, L., Zheng, J., Li, S., 2015. Copper isotopic composition of the silicate Earth. *Earth Planet. Sci. Lett.* 427, 95–103.
- Lodders, K., 2003. Solar system abundances and condensation temperatures of the elements. *The Astrophys. J.* 591, 1220–1247.
- Lowell, J.D., Guilbert, J.M., 1970. Lateral and vertical alteration-mineralization zoning in porphyry ore deposits. *Econ. Geol.* 65, 373–408.
- Luck, J., Othman, D.B., Barrat, J., Albarède, F., 2003. Coupled <sup>63</sup>Cu and <sup>16</sup>O excesses in chondrites. *Geochim. Cosmochim. Acta* 67, 143–151.
- Lv, Y., Liu, S.A., Zhu, J.M., Li, S., 2016. Copper and zinc isotope fractionation during deposition and weathering of highly metalliferous black shales in central China. *Chem. Geol.* 422, 82–93.
- Maher, K.C., Larson, P.B., 2007. Variation in copper isotope ratios and controls on fractionation in hypogene skarn mineralization at Corocchhuayco and Tintaya, Peru. *Econ. Geol.* 102, 225–237.
- Maher, K.C., Jackson, S., Mountain, B., 2011. Experimental evaluation of the fluid–mineral fractionation of Cu isotopes at 250 °C and 300 °C. *Chem. Geol.* 286, 229–239.
- Malitch, K.N., Latypov, R.M., Badanina, I.Y., Sluzhenikin, S.F., 2014. Insights into ore genesis of Ni–Cu–PGE sulfide deposits of the Noril'sk Province (Russia): evidence from copper and sulfur isotopes. *Lithos* 204, 172–187.
- Mao, J., Pirajno, F., Lehmann, B., Luo, M., Berzina, A., 2014. Distribution of porphyry deposits in the Eurasian continent and their corresponding tectonic settings. *J. Asian Earth Sci.* 79, 576–584.
- Maréchal, C.N., Télouk, P., Albarède, F., 1999. Precise analysis of copper and zinc isotopic compositions by plasma-source mass spectrometry. *Chem. Geol.* 156, 251–273.
- Markl, G., Lahaye, Y., Schwinn, G., 2006. Copper isotopes as monitors of redox processes in hydrothermal mineralization. *Geochim. Cosmochim. Acta* 70, 4215–4228.
- Mason, T.F., Weiss, D.J., Chapman, J.B., Wilkinson, J.J., Tessalina, S.G., Spiro, B., Horstwood, M.S., Spratt, J., Coles, B.J., 2005. Zn and Cu isotopic variability in the Alexandrinka volcanic-hosted massive sulphide (VHMS) ore deposit, Urals, Russia. *Chem. Geol.* 221, 170–187.
- Mathur, R., Ruiz, J., Titley, S., Liermann, L., Buss, H., Brantley, S., 2005. Cu isotopic fractionation in the supergene environment with and without bacteria. *Geochim. Cosmochim. Acta* 69, 5233–5246.
- Mathur, R., Titley, S., Barra, F., Brantley, S., Wilson, M., Phillips, A., Munizaga, F., Maksaei, V., Vervoort, J., Hart, G., 2009. Exploration potential of Cu isotope fractionation in porphyry copper deposits. *J. Geochem. Explor.* 102, 1–6.
- Mathur, R., Ruiz, J., Casselman, M.J., Megaw, P., van Egmond, R., 2012. Use of Cu isotopes to distinguish primary and secondary Cu mineralization in the Cañariaco Norte porphyry copper deposit, Northern Peru. *Mineral. Deposita* 47, 755–762.
- Mathur, R., Munk, L., Nguyen, M., Gregory, M., Annell, H., Lang, J., 2013. Modern and Paleofluid Pathways Revealed by Cu Isotope Compositions in Surface Waters and Ores of the Pebble Porphyry Cu–Au–Mo Deposit, Alaska. *Econ. Geol.* 108, 529–541.
- Mo, X., Niu, Y., Dong, G., Zhao, Z., Hou, Z., Zhou, S., Ke, S., 2008. Contribution of syn-collisional felsic magmatism to continental crust growth: A case study of the Paleogene Linzizong volcanic Succession in southern Tibet. *Chem. Geol.* 250, 49–67.
- Mountain, B., Seward, T., 1999. The hydrosulphide/sulphide complexes of copper (I): Experimental determination of stoichiometry and stability at 22 °C and reassessment of high temperature data. *Geochim. Cosmochim. Acta* 63, 11–29.
- Mountain, B., Seward, T., 2003. Hydrosulphide/sulfide complexes of copper (I): experimental confirmation of the stoichiometry and stability of Cu(HS)<sup>2-</sup> to elevated temperatures. *Geochim. Cosmochim. Acta* 67, 3005–3014.
- Pearce, C.I., Patrick, R.A.D., Vaughan, D.J., Henderson, C.M.B., van der Laan, G., 2006. Copper oxidation state in chalcopyrite: Mixed Cu d<sup>9</sup> and d<sup>10</sup> characteristics. *Geochim. Cosmochim. Acta* 70, 4635–4642.
- Pokrovski, G.S., Borisova, A.Y., Harrichoury, J.C., 2008. The effect of sulfur on vapor–liquid fractionation of metals in hydrothermal systems. *Earth Planet. Sci. Lett.* 266, 345–362.
- Qu, X., Hou, Z., Khin, Z., Li, Y., 2007. Characteristics and genesis of Gangdese porphyry copper deposits in the southern Tibetan Plateau: preliminary geochemical and

- geochronological results. *Ore Geol. Rev.* 31, 205–223.
- Rouxel, O., Fouquet, Y., Ludden, J.N., 2004. Copper isotope systematics of the Lucky Strike, Rainbow, and Logatchev sea-floor hydrothermal fields on the Mid-Atlantic Ridge. *Econ. Geol.* 99, 585–600.
- Seo, J.H., Lee, S.K., Lee, I., 2007. Quantum chemical calculations of equilibrium copper (I) isotope fractionations in ore-forming fluids. *Chem. Geol.* 243, 225–237.
- Seo, J.H., Guillong, M., Heinrich, C.A., 2009. The role of sulfur in the formation of magmatic-hydrothermal copper-gold deposits. *Earth Planet. Sci. Lett.* 282, 323–328.
- Sillitoe, R.H., 2010. Porphyry copper systems. *Econ. Geol.* 105, 3–41.
- Simon, A.C., Pettke, T., Candela, P.A., Piccoli, P.M., Heinrich, C.A., 2006. Copper partitioning in a melt-vapor-brine-magnetite-pyrrhotite assemblage. *Geochim. Cosmochim. Acta* 70, 5583–5600.
- Singer, D.A., Berger, V.I., Moring, B.C., 2005. Porphyry copper deposits of the world: database, map, and grade and tonnage models. U.S. Geological Survey Open file report 2005–1060, (<http://pubs.usgs.gov/of/2005/1060/>).
- Sossi, P.A., Halverson, G.P., Nebel, O., Eggins, S.M., 2015. Combined separation of Cu, Fe and Zn from rock matrices and improved analytical protocols for stable isotope determination. *Geostand. Geoanal. Res.* 39, 12–149.
- Sun, X., Zheng, Y., Wu, S., You, Z., Wu, X., Li, M., Zhou, T., Dong, J., 2013. Mineralization age and petrogenesis of associated intrusions in the Mingze-Chengba porphyry-skarn Mo-Cu deposit, Gangdese. *Acta Petrol. Sin.* 29, 1392–1406 (in Chinese with English abstract).
- Sun, X., Zheng, Y., Xu, J., Huang, L., Guo, F., Gao, S., 2017. Metallogenesis and ore controls of Cenozoic porphyry Mo deposits in the Gangdese belt of southern Tibet. *Ore Geol. Rev.* 81, 996–1014.
- Wang, B.D., Xu, J.F., Chen, J.L., Zhang, X.G., Wang, L.Q., Xia, B.B., 2010. Petrogenesis and geochronology of the ore-bearing porphyritic rocks in Tangbula porphyry molybdenum-copper deposit in the eastern segment of the Gangdese metallogenic belt. *Acta Petrol. Sin.* 26, 1820–1832 (in Chinese with English abstract).
- Wang, P., Dong, G.C., Santosh, M., Liu, K.R., Li, X.F., 2017. Copper isotopes trace the evolution of skarn ores: a case study from the Hongshan-Hongniu Cu deposit, southwest China. *Ore Geol. Rev.* 88, 822–831.
- Weinstein, C., Moynier, F., Wang, K., Paniello, R., Foriel, J., Catalano, J., Pichat, S., 2011. Isotopic fractionation of Cu in plants. *Chem. Geol.* 286, 266–271.
- Wen, D.R., Chung, S.L., Song, B., Iizuka, Y., Yang, H.J., Ji, J., Liu, D., Gallet, S., 2008. Late Cretaceous Gangdese intrusions of adakitic geochemical characteristics, SE Tibet: petrogenesis and tectonic implications. *Lithos* 105, 1–11.
- Williams-Jones, A.E., Heinrich, C.A., 2005. 100th Anniversary special paper: vapor transport of metals and the formation of magmatic-hydrothermal ore deposits. *Econ. Geol.* 100, 1287–1312.
- Wu, S., Zheng, Y.Y., Sun, X., Liu, S.A., Geng, R.R., You, Z.M., Ouyang, H.T., Lei, D., Zhao, Z.Y., 2014. Origin of the Miocene porphyries and their mafic microgranular enclaves from Dabu porphyry Cu-Mo deposit, southern Tibet: implications for magma mixing/mingling and mineralization. *Int. Geol. Rev.* 56, 571–595.
- Wu, S., Zheng, Y.Y., Sun, X., 2016. Subduction metasomatism and collision-related metamorphic dehydration controls on the fertility of porphyry copper ore-forming high Sr/Y magma in Tibet. *Ore Geol. Rev.* 73, 83–103.
- Wu, S., Zheng, Y., Geng, R., Jin, L., Bao, B., Tan, M., Guo, F., 2017a. Geology, fluid inclusion and isotope constraints on ore genesis of the post-collisional Dabu porphyry Cu-Mo deposit, southern Tibet. *Ore Geol. Rev.* 89, 421–440.
- Wu, L.Y., Hu, R.Z., Li, X.F., Liu, S.A., Tang, Y.W., Tang, Y.Y., 2017b. Copper isotopic compositions of the Zijinshan high-sulfidation epithermal Cu-Au deposit, South China: Implications for deposit origin. *Ore Geol. Rev.* 83, 191–199.
- Yao, J., Mathur, R., Sun, W., Song, W., Chen, H., Mutti, L., Xiang, X., Luo, X., 2016. Fractionation of Cu and Mo isotopes caused by vapor-liquid partitioning, evidence from the Dahutang W-Cu-Mo deposit. *Geochem. Geophys. Geosyst.* 17, 1725–1739.
- Zhao, Y., Xue, C., Liu, S.-A., Symons, D.T.A., Zhao, X., Yang, Y., Ke, J., 2017. Copper isotope fractionation during sulfide-magma differentiation in the Tulaergen magmatic Ni-Cu deposit, NW China. *Lithos* 286–287, 206–215.
- Zheng, Y.Y., Xue, Y.X., Cheng, L.J., Fan, Z.H., Gao, S.B., 2004. Finding, characteristics and significances of qulong superlarge porphyry copper(Molybdenum) Deposit, Tibet. *Earth Sci.* 29, 103–108 (in Chinese with English abstract).
- Zheng, Y.C., Hou, Z.Q., Li, W., Liang, W., Huang, K.X., Li, Q.Y., Sun, Q.Z., Fu, Q., Zhang, S., 2012. Petrogenesis and Geological Implications of the Oligocene Chongmuda-Mingze Adakite-Like Intrusions and Their Mafic Enclaves, Southern Tibet. *J. Geol.* 120, 647–669.
- Zheng, Y., Sun, X., Gao, S., Wang, C., Zhao, Z., Wu, S., Li, J., Wu, X., 2014a. Analysis of stream sediment data for exploring the Zhunuo porphyry Cu deposit, southern Tibet. *J. Geochem. Explor.* 143, 19–30.
- Zheng, Y., Sun, X., Gao, S., Zhao, Z., Zhang, G., Wu, S., You, Z., Li, J., 2014b. Multiple mineralization events at the Jiru porphyry copper deposit, southern Tibet: Implications for Eocene and Miocene magma sources and resource potential. *J. Asian Earth Sci.* 79, 842–857.
- Zheng, Y., Sun, X., Gao, S., Wu, S., Xu, J., Jiang, J., Chen, X., Zhao, Z., Liu, Y., 2015. Metallogenesis and the minerogenetic series in the Gangdese polymetallic copper belt. *J. Asian Earth Sci.* 103, 23–39.
- Zhu, X.K., O'Nions, R.K., Guo, Y., Belshaw, N.S., Rickard, D., 2000. Determination of natural Cu-isotope variation by plasma-source mass spectrometry: implications for use as geochemical tracers. *Chem. Geol.* 163, 139–149.